ChemComm

ROYAL SOCIETY OF CHEMISTRY

COMMUNICATION

Cite this: *Chem. Commun.*, 2022, **58**, 1143

Received 13th September 2021,
Accepted 19th December 2021

DOI: 10.1039/d1cc05139c

rsc.li/chemcomm

Electrocatalytic H_2 evolution promoted by a bioinspired (N2S2)Ni(II) complex†

Soumalya Sinha, ‡ Giang N. Tran, ‡ Hanah Na and Liviu M. Mirica *

A bioinspired (N2S2)Ni(II) electrocatalyst is reported that produces H_2 from CF_3CO_2H with a turnover frequency (TOF) of ~1250 s^{-1} at low acid concentration (<0.043 M) in MeCN. A mechanism for the H_2 production by this electrocatalyst is proposed and its activity is benchmarked against those of other reported molecular Ni H_2 evolution electrocatalysts. The involvement of a hemilabile pyridyl group of the N2S2 ligand is proposed to mimic the role of a cysteine residue involved in the biological proton reduction performed by [NiFe] hydrogenases.

Hydrogen (H_2) is a key ingredient for employing renewable energy sources on a larger scale.[1] The primary challenge of such technologies is to implement earth-abundant materials to produce H_2 with high turnover frequency (TOF). Biological catalysts such as [NiFe] hydrogenases that exhibit TOFs of ~1000 sec^{-1} under weak acidic conditions have been the inspiration for reducing H^+ to H_2.[2] The H^+ transfer events occur at the Ni center, which is bound to two terminal cysteine (Cys) groups and two bridging Cys thiolates. The key species in the HER catalytic cycle is the Ni-R state that releases H_2 and returns to the resting state Ni-SIa (Fig. 1).[3]

Although structural mimics of [NiFe] hydrogenases have been reported, their performance in catalytic HER is either not described or kinetically sluggish.[4] Furthermore, there are other efficient mononuclear Ni complexes reported for electrocatalytic HER. For example, DuBois *et al.* reported Ni phosphine complexes that feature flexible amine arms as proton relay groups and perform HER using a strong acid, protonated dimethylformamide ($[DMF–H]^+$, pK_a = 6.1 in MeCN).[5] Later, DuBois *et al.* and Dempsey *et al.* investigated the electrochemical HER mechanism of such Ni phosphine complexes and showed that the flexible amine arms do not interact with the Ni center, yet they only shuttle protons through H-bonding.[6] A common drawback for these molecular HER electrocatalysts is the use of strong acids and often at high concentrations in non-aqueous electrolytes to achieve high TOFs.

A few reported molecular Ni^{II} electrocatalysts perform HER at low overpotential using weak acids. Jones *et al.* reported a S_2P_2-coordinated Ni HER electrocatalyst, which produces H_2 from CH_3CO_2H (AcOH, pK_a = 22.48 in THF) at only 240 mV of overpotential, yet with a low TOF of 1240 s^{-1}.[7] In addition, a Ni complex bearing phosphinopyridyl ligands with amine residues showed comparatively higher TOF of 8400 s^{-1} using AcOH in MeCN (pK_a = 23.51), but at a high overpotential (590 mV).[8]

Herein, we report the synthesis and characterization of a bioinspired Ni complex $[(N2S2)Ni^{II}(MeCN)_2](OTf)_2$, **1·(OTf)$_2$**, where N2S2 is 3,7-dithia-1,5(2,6)-dipyridinacyclooctaphane (Fig. 2). We then studied the electrocatalytic HER reactivity of $\mathbf{1}^{2+}$ in MeCN using the acids CF_3CO_2H (TFA, pK_a = 12.65)[9] or AcOH as the proton sources. Remarkably, $\mathbf{1}^{2+}$ showed HER electrocatalytic activity with a TOF of ~1250 s^{-1} using only 0.043 M of TFA in MeCN with ≤2 M H_2O. We attribute such elevated performance of $\mathbf{1}^{2+}$ at low acid concentrations to the role of one of the pyridyl group of N2S2 in proton binding and transfer events during HER. Our previous studies have shown that the N2S2 ligand is conformationally flexible and can adopt k^2, k^3, and k^4 binding modes, depending on the geometric preference of the metal center.[10] Thus, the 'hemilabile' nature of the pyridyl group in N2S2 that can act as both a ligand and a proton relay can be viewed as mimicking the role of Cys residues in [NiFe] hydrogenases.[11]

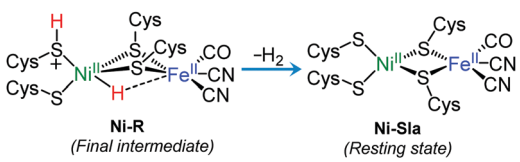

Fig. 1 The final step observed in [NiFe] hydrogenases catalyzed the HER cycle.

Department of Chemistry University of Illinois at Urbana Champaign 600 S. Mathews Avenue, Urbana, Illinois 61801, USA. E-mail: mirica@illinois.edu

† Electronic supplementary information (ESI) available. CCDC 2053835. For ESI and crystallographic data in CIF or other electronic format see DOI: 10.1039/d1cc05139c

‡ These authors contributed equally.

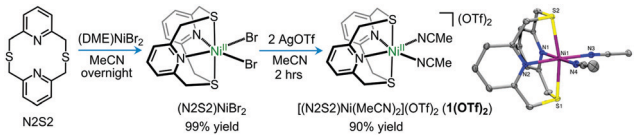

Fig. 2 Synthetic scheme for [(N2S2)Ni(MeCN)2](OTf)2 (**1·(OTf)$_2$**) and ORTEP representation (50% probability ellipsoids) for $\mathbf{1}^{2+}$. Selected bond distances (Å): Ni1–N1 2.071(9), Ni1–N2 2.060(10), Ni1–S1 2.379(3), Ni1–S2 2.394(3), Ni1–N3 2.060(10), Ni1–N4 2.039(10).

The N2S2 ligand was prepared following a slightly modified literature procedure, and **1·(OTf)$_2$** was synthesized as a purple solid in up to 90% yield.[12] Single crystal X-ray analysis of **1·(OTf)$_2$** reveals a tetragonally distorted octahedral coordination of the Ni^{II} center, with the two N atoms of the N2S2 ligand and two MeCN molecules occupying the equatorial positions, with an average Ni–N bond distance of 2.06 Å (Fig. 2). The two S atoms of N2S2 occupy the axial positions with longer average Ni–S bond lengths of 2.386 Å, thus completing a κ^4 binding mode for the N2S2 ligand.

We then studied the electrochemical behavior of $\mathbf{1}^{2+}$ in N_2-saturated 0.1 M $^nBu_4NPF_6$ (TBAP)/MeCN. The cyclic voltammograms (CVs) of $\mathbf{1}^{2+}$ showed a quasi-reversible redox wave centered at −1.30 V *vs.* $Fc^{+/0}$ and an irreversible wave at −1.75 V *vs.* $Fc^{+/0}$, assigned to the $Ni^{II/I}$ and $Ni^{I/0}$ redox couples, respectively (Fig. S5a, ESI†).[12] Variable scan rate CVs confirmed diffusion-controlled electrochemical processes by exhibiting a linear correlation between the cathodic peak currents and the square root of the scan rates (Fig. S5b and S6, ESI†).[13]

The electrochemical HER activity of $\mathbf{1}^{2+}$ was first tested using AcOH as the acid. The addition of AcOH showed an increase in the peak current densities at potentials lower than −2 V (Fig. S7, ESI†), yet the current enhancement for $\mathbf{1}^{2+}$ overlapped with the background electrode contribution (Fig. S11, ESI†). A stronger acid, TFA, was then chosen, and the CVs recorded for $\mathbf{1}^{2+}$ in the presence of TFA exhibit catalytic current enhancement for two cathodic peak potentials, $E_{pc}^{(1)}$ and $E_{pc}^{(2)}$, and the peak current densities increased as the concentration of TFA was increased up to 43.41 mM (Fig. 3). The onset potentials of these catalytic CVs were at least 500 mV more positive than the $Ni^{II/I}$ reduction potential $E_{Ni(II/I)}$. Additionally, the catalytic peak potentials (E_{cat}) were ≥365 mV more positive than that of GC-promoted HER in the absence of $\mathbf{1}^{2+}$ (Fig. S12, ESI†).

To investigate the HER process catalyzed by $\mathbf{1}^{2+}$, the shift in $E_{pc}^{(1)}$ was plotted *vs.* log[TFA] and fitted linearly to yield a slope of 23 mV dec^{-1} (Fig. 4a, blue dots), indicating a typical EC-type electrochemical mechanism, where E is the Nernstian e^- transfer, followed by an irreversible chemical (C) step.[13] The catalytic peak currents did not plateau upon the further increase in TFA concentration (>0.043 M). Therefore the Randles–Sevcik equation cannot be applied to obtain the catalytic rate constant. Instead, foot-of-the-wave analysis (FOWA) was used to estimate the rate constants (k_{FOWA}, Table S1, ESI†) for the C step (the first protonation step) at different TFA concentrations by subtracting the background currents observed for the bare GC electrode under identical electrochemical conditions (Fig. S16, ESI†).[9] The log(k_{FOWA}) values were plotted *vs.* log[TFA] and a slope of 1.5 was obtained (Fig. 4b), suggesting the order of the reaction in acid is greater than 1.

Based on these results, we propose a catalytic HER mechanism in which $\mathbf{1}^{2+}$ undergoes two sequential e^- reduction steps to generate the Ni^0 species **1** (Fig. 5). The protonation (the C step) of **1** can generate **2**, which is tentatively assigned as a (N2S2)Ni^{II}–H species. We propose that **2** adopts a square planar geometry where the non-chelating pyridyl group can get protonated or create a hydrogen bond with a TFA molecule, which may explain the greater than 1 order of the reaction in TFA. Furthermore, the protonation of the pyridyl group in the next step could yield **3** that can release H_2 and regenerate $\mathbf{1}^{2+}$ upon solvation. Since the pK_a of TFA is 12.65 in MeCN,[14] while the pK_a of pyridinium is 12.53 in MeCN,[15] it is expected that TFA could protonate one of the pyridyl group in N2S2 even in the presence of a metal ion. Therefore, the pyridyl group of N2S2 could be viewed as mimicking the Cys residue in the Ni-R state of [NiFe] hydrogenase that can shuttle between a metal-bound state and a protonated state during the HER catalytic cycle.[11]

To evaluate the effect of H_2O on HER catalysis, we employed a 0.043 M TFA in MeCN and three different H_2O concentrations (1.0 M, 1.5 M, and 2.0 M). Linear sweep voltammograms (LSVs) recorded for $\mathbf{1}^{2+}$ under these conditions show plateau currents at potentials lower than −1.75 V, and the shape of the LSVs remained unchanged as more H_2O was added (Fig. 6).

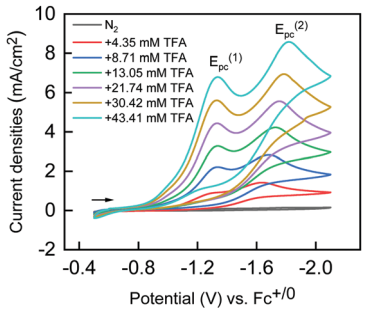

Fig. 3 CVs of $\mathbf{1}^{2+}$ (1 mM) without (black) and with different concentrations of TFA (4.35–43.41 mM) in N_2-saturated 0.1 M TBAP/MeCN. $E_{pc}^{(1)}$ and $E_{pc}^{(2)}$ indicate the first and second cathodic peak potentials, respectively. Scan rate = 0.1 V s^{-1}.

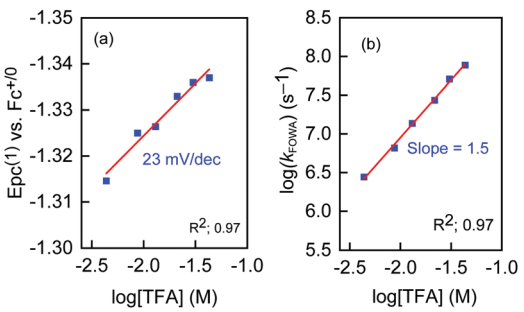

Fig. 4 (a) Plot of first reductive peak potentials, $E_{pc}^{(1)}$ at different TFA conc. *vs.* logarithm of [TFA], 4.35–43.41 mM (blue dots). (b) Plot of the logarithm of k_{FOWA} obtained from FOWA *vs.* logarithm of [TFA] within the same concentration range as used in (a).

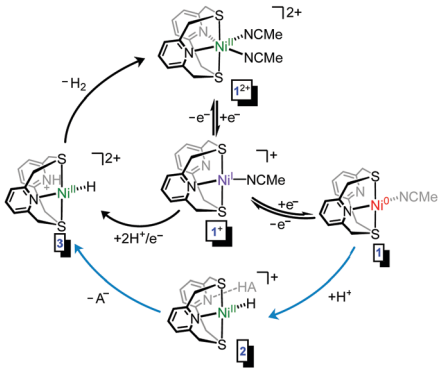

Fig. 5 Proposed catalytic HER cycle (black arrows) for $\mathbf{1}^{2+}$. The blue arrows include the possible intermediate. HA = TFA.

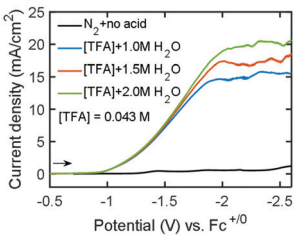

Fig. 6 Linear sweep voltammograms for $\mathbf{1}^{2+}$ recorded in N_2-saturated 0.1 M TBAP/MeCN in the absence of TFA (black) and the presence of 0.043 M TFA + different concentration of H_2O, 1 M (blue), 1.5 M (orange), and 2.0 M (green). Scan rate = 0.1 V s^{-1}.

FOWA was then carried out and the average reaction rate constant for the first C step ($k_{FOWA,avg}$) determined for $\mathbf{1}^{2+}$ is 1.95×10^5 s^{-1} (Fig. S18a and Table S2, ESI†).[12] Notably, this rate constant is independent of the H_2O concentration (Fig. S18b, ESI†), and thus the role of H_2O can be described as mainly impeding the homoconjugation of TFA in MeCN, without interfering with the thermodynamic parameters.[9] Overall, we posit that **3** can produce H_2 mediated by the protonation of the pyridyl group of N2S2, which is less sensitive to how acidic the bulk electrolyte is. Since the FOWA plots deviate from linearity at potentials more negative than −1.6 V, the TOFs determined based on $k_{FOWA,\ avg}$ may significantly overestimate the rate constant at the rate-determining step.[9,16] Herein, we used eqn (1),[5b] where i_{cat} is the catalytic current density at the plateau current in the presence of 0.043 M of TFA + 2 M H_2O, i_p is the peak current density at the $Ni^{II/I}$ reduction with no acids, and ν is the scan rate (0.1 V s^{-1}), to obtain a catalytic rate constant (k_{obs}) or TOF of ~1250 s^{-1}.

$$k_{obs} = 1.94\ V^{-1} \times \nu \times (i_{cat}/i_p)^2; \quad (1)$$

The overpotential for the HER process calculated using the Appel and Helm method[17] was found to be 730 mV at $E_{cat/2}$ for $\mathbf{1}^{2+}$ in the presence of 0.043 M TFA with 1.5 M H_2O in MeCN. Chronoamperometric experiments carried out for $\mathbf{1}^{2+}$ showed a total charge of 200 mC passed over 15 mins of electrolysis at an applied potential of $E_{cat/2}$, corresponding to 1.03×10^{-6} moles of H_2 (Fig. S13, ESI†). Bulk electrolysis for $\mathbf{1}^{2+}$ was then performed at $E_{cat/2}$ using a carbon cloth electrode and 0.186 mmoles H_2 were detected by GC (Fig. S15, ESI†), corresponding to a faradaic efficiency (FE) of 92%. Importantly, complex $\mathbf{1}^{2+}$ was stable during electrolysis, and no color change or formation of precipitate were observed during electrocatalysis, while the CV of the post-electrolysis solution was similar to the CV of $\mathbf{1}^{2+}$ in presence of TFA.

While TFA is a fairly strong acid in MeCN and bare carbon electrodes can perform HER using only TFA at potentials lower than −1 V,[9] the average currents obtained for $\mathbf{1}^{2+}$ during bulk electrolysis were much higher than the background contribution (Fig. S14, ESI†). The background charge passed during the electrocatalytic HER process in the presence of the bare electrode is about 30% *vs.* the charge passed in the presence of $\mathbf{1}^{2+}$, yet the FE of the background HER process is low (<25%) and does not contribute to more than 10% of the total H_2 produced (Fig. S15, ESI†). Finally, the HER activity of the rinsed post-electrolysis electrode was identical to that of a clean glassy carbon electrode under the same electrolysis conditions, suggesting that the probed HER process is mainly homogeneous in nature.

To benchmark the HER activity of $\mathbf{1}^{2+}$, we selected five efficient Ni^{II}-based HER electrocatalysts, **4**,[7] $\mathbf{5}^{2+}$,[8] $\mathbf{6}^{2+}$,[5a] $\mathbf{7}^{2+}$,[5b] and $\mathbf{8}^{2+}$ (Fig. 7a).[6a,18] We have included the reported TOF values for these electrocatalysts and calculated the overpotentials by correcting the standard thermodynamic potentials (E_{HA}) for H^+-to-H_2 conversion at the given pK_a of the acid (HA) used in the corresponding non-aqueous electrolyte (eqn (2)).[9]

$$E_{HA} = E^0 - (2.303RT/F) \times pK_a\ (HA); \quad (2)$$

The logTOF values were then plotted *vs.* the calculated overpotentials ($E^0 - E_{HA}$) for the Ni complexes mentioned above and $\mathbf{1}^{2+}$ (Fig. 7b). Remarkably, $\mathbf{1}^{2+}$ performs electrocatalytic HER at a higher TOF than those of **4** and $\mathbf{8}^{2+}$, where **4** used 0.05 M of AcOH in THF[7] and $\mathbf{8}^{2+}$ required ≤0.6 M of the strong acid anilinium (pK_a = 10.62 in MeCN)[6a,9] or 0.25 M of $[(DMF)H]^+$ in MeCN.[18] While the overpotential for $\mathbf{1}^{2+}$ is higher than those

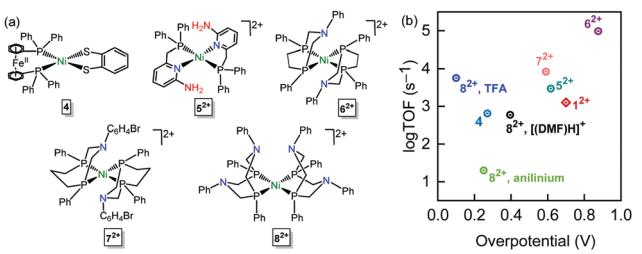

Fig. 7 (a) Selected Ni^{II} HER electrocatalysts reported for efficient HER: **4**,[7] $\mathbf{5}^{2+}$,[8] $\mathbf{6}^{2+}$,[5a] $\mathbf{7}^{2+}$,[5b] and $\mathbf{8}^{2+}$.[6a,18] (b) Comparison of the logarithm of TOF *vs.* the calculated overpotential reported for the Ni electrocatalysts shown in (a) and $\mathbf{1}^{2+}$. The proton sources used are: 0.043 M TFA + 2 M H_2O in MeCN for $\mathbf{1}^{2+}$, 0.05 M AcOH in THF for **4**, 0.3 M AcOH in MeCN for $\mathbf{5}^{2+}$, 0.42 M $[(DMF)H]^+$ + 1.2 M H_2O in MeCN for $\mathbf{6}^{2+}$, 1.26 M $[(DMF)H]^+$ + 1.09 M H_2O in MeCN for $\mathbf{7}^{2+}$. For $\mathbf{8}^{2+}$, 0.6 M anilinium,[6a] 0.25 M $[(DMF)H]^+$, or 1.8 M TFA in MeCN.[18]

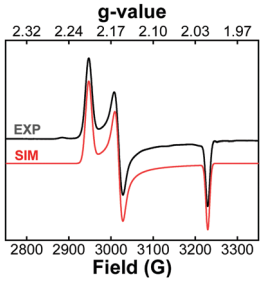

Fig. 8 Experimental (black) and simulated (red) EPR spectra for $\mathbf{1}^{2+}$ after treating it with 1 equiv. of $CoCp_2^*$ in 1 : 3 MeCN:PrCN glass at 77 K. The following g values were used for the simulation: g_x = 2.205, g_y = 2.152, g_z = 2.012.

of **4**, $\mathbf{5}^{2+}$, $\mathbf{7}^{2+}$, and $\mathbf{8}^{2+}$, it is lower than that for $\mathbf{6}^{2+}$, albeit $\mathbf{6}^{2+}$ employs the strong acid $[(DMF)H]^+$ at concentrations >0.4 M. Overall, the electrochemical HER performance of $\mathbf{1}^{2+}$ is significant, especially since competitive HER kinetics can be achieved at low acid concentration using a weaker acid. The only other Ni HER electrocatalysts containing thiolate and/or pyridine ligands, **4** and $\mathbf{5}^{2+}$, exhibit TOFs that are comparable to that of $\mathbf{1}^{2+}$.

We also performed electron paramagnetic resonance (EPR) spectroscopy to detect a Ni^I species upon reducing $\mathbf{1}^{2+}$ with 1 equiv. of $CoCp^*_2$ (Cp* = pentamethylcyclopentadienyl). The X-band EPR spectrum of the reduced $\mathbf{1}^{2+}$ in 1 : 3 MeCN:PrCN (v/v) at 77 K (Fig. 8) simulated using a rhombic g tensor (g_x = 2.205, g_y = 2.152, g_z = 2.012). We attribute this EPR signal to a $(N2S2)Ni^I$ species $\mathbf{1}^+$, suggesting a $d_{x^2-y^2}$ ground state in a square planar geometry, similar to other reported Ni^I complexes,[19] although the formation of a Ni^{III} species *in situ via* an oxidative process cannot be excluded. Intriguingly, the addition of 1 equiv. TFA to the *in situ* generated $\mathbf{1}^+$ led to an immediate disappearance of the corresponding EPR signal, further supporting the proposed mechanism in which $\mathbf{1}^{2+}$ can be reduced chemically/electrochemically to generate $\mathbf{1}^+$, which is reactive toward protons in an organic solvent (Fig. 5).

In summary, we report a bioinspired complex $[(N2S2)Ni(MeCN)_2]^{2+}$, $\mathbf{1}^{2+}$, that is an efficient HER electrocatalyst and reduces protons to H_2 at low acid concentrations. Given that most of the reported Ni-based molecular HER electrocatalysts perform HER using stronger acids than TFA, and often at high acid concentrations,[5,6] the performance of $\mathbf{1}^{2+}$ is remarkable. In addition, we highlight the role of the pendant pyridyl group of the N2S2 ligand in leading to elevated HER kinetics, which resembles the proton-relay role of the Cys residue in [NiFe] hydrogenases that can shuttle between a metal-bound and a protonated state. Although $\mathbf{1}^{2+}$ catalyzes the HER process at a high overpotential, 0.7 V, the proposed HER mechanism should inspire the development of improved bioinspired HER electrocatalysts that operate under benign reaction conditions.

We thank the Department of Energy's BES Catalysis Science Program (DE-SC0006862) for support of the initial work, and the National Science Foundation (CHE-1925751) for the support of the subsequent work. We thank Prof. Nigam P. Rath (Univ. of Missouri) for obtaining the crystal structure of $\mathbf{1}\cdot(OTf)_2$, and the research facilities at the Univ. of Illinois at Urbana-Champaign for assistance.

Conflicts of interest

There are no conflicts to declare.

Notes and references

1 N. S. Lewis and D. G. Nocera, *Proc. Natl. Acad. Sci. U. S. A.*, 2006, **103**, 15729–15735.
2 (*a*) F. A. Armstrong, *Curr. Opin. Chem. Biol.*, 2004, **8**, 133–140; (*b*) H. S. Shafaat, in *Comprehensive Coordination Chemistry III*, ed. E. C. Constable, G. Parkin and L. Que Jr, Elsevier, Oxford, 2021, pp. 707–730.
3 (*a*) W. Lubitz, H. Ogata, O. Rüdiger and E. Reijerse, *Chem. Rev.*, 2014, **114**, 4081–4148; (*b*) T. Xu, D. Chen and X. Hu, *Coord. Chem. Rev.*, 2015, **303**, 32–41.
4 (*a*) Y. Ohki, K. Yasumura, K. Kuge, S. Tanino, M. Ando, Z. Li and K. Tatsumi, *Proc. Natl. Acad. Sci. U. S. A.*, 2008, **105**, 7652; (*b*) S. Canaguier, M. Field, Y. Oudart, J. Pécaut, M. Fontecave and V. Artero, *Chem. Commun.*, 2010, **46**, 5876–5878; (*c*) M. E. Ahmed and A. Dey, *Curr. Opin. Electrochem.*, 2019, **15**, 155–164.
5 (*a*) M. L. Helm, M. P. Stewart, R. M. Bullock, M. R. DuBois and D. L. DuBois, *Science*, 2011, **333**, 863–866; (*b*) S. Wiese, U. J. Kilgore, M.-H. Ho, S. Raugei, D. L. DuBois, R. M. Bullock and M. L. Helm, *ACS Catal.*, 2013, **3**, 2527–2535.
6 (*a*) E. S. Rountree and J. L. Dempsey, *J. Am. Chem. Soc.*, 2015, **137**, 13371–13380; (*b*) D. L. DuBois, *Inorg. Chem.*, 2014, **53**, 3935–3960.
7 L. Gan, T. L. Groy, P. Tarakeshwar, S. K. Mazinani, J. Shearer, V. Mujica and A. K. Jones, *J. Am. Chem. Soc.*, 2015, **137**, 1109–1115.
8 R. Tatematsu, T. Inomata, T. Ozawa and H. Masuda, *Angew. Chem., Int. Ed.*, 2016, **55**, 5247–5250.
9 B. D. McCarthy, D. J. Martin, E. S. Rountree, A. C. Ullman and J. L. Dempsey, *Inorg. Chem.*, 2014, **53**, 8350–8361.
10 (*a*) J. Luo, J. R. Khusnutdinova, N. P. Rath and L. M. Mirica, *Chem. Commun.*, 2012, **48**, 1532–1534; (*b*) J. Luo, N. P. Rath and L. M. Mirica, *Organometallics*, 2013, **31**, 3343–3353; (*c*) J. Luo, G. N. Tran, N. P. Rath and L. M. Mirica, *Inorg. Chem.*, 2020, **59**, 15659–15669.
11 S. Ding, P. Ghosh, M. Y. Darensbourg and M. B. Hall, *Proc. Natl. Acad. Sci. U. S. A.*, 2017, **114**, E9775.
12 See Supporting Information.
13 A. J. Bard and L. R. Faulkner, *Electrochemical methods: Fundamentals and applications*, Wiley, 2001.
14 F. Eckert, I. Leito, I. Kaljurand, A. Kütt, A. Klamt and M. Diedenhofen, *J. Comput. Chem.*, 2009, **30**, 799–810.
15 A. Kütt, S. Tshepelevitsh, J. Saame, M. Lõkov, I. Kaljurand, S. Selberg and I. Leito, *Eur. J. Org. Chem.*, 2021, 1407–1419.
16 (*a*) E. S. WiednerH. J. S. BrownM. L. HelmJ. Am. Chem. Soc.138–616; (*b*) V. C. C. Wang and B. A. Johnson, *ACS Catal.*, 2019, **9**, 7109–7123.
17 A. M. Appel and M. L. Helm, *ACS Catal.*, 2014, **4**, 630–633.
18 E. S. Wiedner and M. L. Helm, *Organometallics*, 2014, **33**, 4617–4620.
19 C. L. Wagner, G. Herrera, Q. Lin, C. Hu and T. Diao, *J. Am. Chem. Soc.*, 2021, **143**, 5295–5300.

